Detailed study and mean field interpretation of $^{16}O+^{12}C$ elastic scattering at seven medium energies

M. P. Nicoli,[1] F. Haas,[1] R. M. Freeman,[1] S. Szilner,[2] Z. Basrak,[2] A. Morsad,[3] G. R. Satchler,[4] and M. E. Brandan[5]
[1]*Institut de Recherches Subatomiques, UMR7500, CNRS-IN2P3 and Université Louis Pasteur, BP28, F-67037 Strasbourg Cedex 2, France*
[2]*Ruđer Bošković Institute, Zagreb, Croatia*
[3]*Faculté des Sciences Ben M'Sik, Université Hassan II, Casablanca, Morroco*
[4]*Department of Physics and Astronomy, University of Tennessee, Knoxville, Tennessee 37996 and Physics Division, Oak Ridge National Laboratory, Oak Ridge, Tennessee 37831-6373*
[5]*Instituto de Física, Universidad Nacional Autónoma de México, Apartado Postal 20-364, México 01000 Distrito Federal, Mexico*
(Received 31 August 1999; published 16 February 2000)

Detailed measurements of the elastic scattering of ^{16}O ions from ^{12}C have been carried out at seven energies from 62 to 124 MeV, at center-of-mass angles from about 10° to about 145°. A coherent optical model analysis of these data has been performed using both the Woods-Saxon and the folding-model potentials. The extracted results are consistent with analyses of data at higher energies for this and similar light heavy-ion systems. Some model-independent spline forms for the real potentials were also investigated.

PACS number(s): 25.70.Bc, 24.10.Ht

I. INTRODUCTION

The last decade has seen significant progress in our understanding of the optical potential that describes the elastic scattering of two light heavy ions. When refractive effects, particularly nuclear rainbows, are discernible, it has been shown that in favorable circumstances one can obtain unambiguous information about the character of the optical potential. The resulting potentials are found to have real parts that are strongly attractive (''deep'') and have imaginary parts that are relatively weakly absorbing. A good understanding of the real potentials has been obtained, based upon the folding model whereby a realistic effective nucleon-nucleon interaction is folded over the density distributions of the two ions. In general, this interaction is also density dependent. The above matters have been reviewed recently [1,2].

Previous studies of refractive effects have concentrated on the symmetrical systems $^{12}C+^{12}C$ and $^{16}O+^{16}O$, where symmetrization results in interferences at the larger angles as one approaches 90°. Consequently, there is value in studying nonidentical systems, such as $^{16}O+^{12}C$, which allow one to explore directly the scattering at larger angles beyond 90°.

Earlier measurements on this reaction have been reported at at $E/A=38$ MeV [3] and $E/A=8.25$ MeV [4]. Both revealed sufficient refractive features in their angular distributions establishing the need for deep real potentials like those found for the symmetrical systems. In the medium energy range between 62 and 124 MeV the present data for $^{16}O+^{12}C$ scattering, whose angular distributions range out to 145° in the center-of-mass system, present the usual diffraction-like behavior at the smaller angles (up to about 50° or 60°) but are then followed by considerable structure at the intermediate and larger angles. Such features are notoriously difficult to reproduce using a simple optical potential. Furthermore, although there do not appear to be measurements of excitation functions available for this system, in this energy range, there are for similar light heavy-ion pairs [5], and these indicate fine structure with respect to bombarding energy up to at least 35 MeV in the center of mass. Indeed, in the case of $^{12}C+^{12}C$, this fine structure (widths of 1 MeV or less) persists up to at least $E_{\mathrm{c.m.}}=60$ MeV [6–8], superimposed upon a gross structure (widths of roughly a few MeV) which can be attributed to refractive effects in the mean field of interaction between the two ions [9]. It is this latter phenomenon that we can hope to explain in terms of a simple optical potential, but the fine structure is also reflected in the observed angular distributions, particularly at the largest angles. Consequently, the problem faced by any analysis of these data is akin to determining their average behavior. This was attempted recently for $^{12}C+^{12}C$ scattering, and we shall follow the philosophy enunciated there [10]. In particular, we show that the type of potentials required by the scattering measurements at higher energies and for similar light heavy-ion systems, can also account for the present data in this average way.

II. EXPERIMENTAL DETAILS

The $^{16}O+^{12}C$ elastic scattering has been measured at $E_{\mathrm{lab}}=62$, 75, 80, 94.8, 100, 115.9, and 124 MeV with an ^{16}O beam provided by the Strasbourg Tandem Vivitron accelerator. The carbon target used in our experiments were self-supporting C films of $\sim 20\ \mu g/cm^2$ thickness.

Detailed and complete angular distributions have been measured at all seven energies. The most forward angles ($5° \leqslant \theta_{\mathrm{lab}} \leqslant 20°$) of a given angular distribution were covered by a Q3D magnetic spectrometer having a proportional counter in its focal plane. The spectrometer measurements were taken in steps of $\Delta\theta_{\mathrm{lab}}=0.5°$. The cross sections at larger angles were measured using a fixed kinematical-coincidence setup composed of two position-sensitive silicon detectors (area$=5\times 1\ cm^2$) placed at 7.8 cm from the target, on both sides of the beam, and covering angles between 15° and 50°, and $-35°$ and $-70°$, respectively. The electronics and data acquisition system of the spectrometer detector and

of the Si detectors were independent from each other. At each bombarding energy, about 50 different measurements were performed at forward angles with the Q3D spectometer while acumulating data in the fixed Si detector setup. The two detector systems had an overlapping angular domain and thus angular distributions of the elastic scattering between $\theta_{cm}=10°$ and 145° could be obtained with good statistics at the seven bombarding energies of this study. All details concerning the data analysis, in particular the identification of the elastic channel in both detection systems, and the extraction of cross section can be found in the thesis of Nicoli [11].

III. OPTICAL MODEL POTENTIALS

The use of a simple optical model potential implies that there are no effects, such as due to the coupling to nonelastic channels, which vary rapidly with energy, or which cannot be represented, at least in an average way, by a local, L-independent potential. These effects could include elastic transfer of an α-particle cluster between the two nuclei. It has been suggested [12] that such a process could be represented by a term in the optical potential that depends upon the parity $(-1)^L$ of the partial waves of relative motion. In particular this could have the effect of increasing the yield at the largest angles and introducing additional structure in the angular distribution. We have no direct evidence of such a process (which is indistinguishable from elastic scattering) and in the present analysis we assume that, if present, it may be subsumed in the properties of the local potential.

Several choices were tried for the real part, $V_E(r)$, of these potentials, as described below. Relatively weak absorption is a characteristic of the potentials for these light heavy ions [2], so that a very helpful measure of the real potential strength is the volume integral per interacting pair,

$$J_V(E)=-\frac{4\pi}{A_1A_2}\int V_E(r)r^2dr. \tag{1}$$

Then one expects the J_V values to be similar for adjacent heavy-ion pairs. Experience suggests that we should find J_V around 300 MeV fm^3 in the present case.

A. Imaginary potentials

We adopted a sum of conventional Woods-Saxon (WS), and the derivative of Woods-Saxon (WSD), forms for the absorptive, imaginary potentials $W(r)$. This is defined by

$$W(r)=-Wf_W(r)-W_Df_D(r), \tag{2}$$

where the ''volume'' (WS) term is

$$f_W(r)=\left[1+\exp\left(\frac{r-R_W}{a_W}\right)\right]^{-1}, \tag{3}$$

while the ''surface'' or derivative (WSD) term is

$$f_D(r)=-4a_Dd/dr\left[1+\exp\left(\frac{r-R_D}{a_D}\right)\right]^{-1}. \tag{4}$$

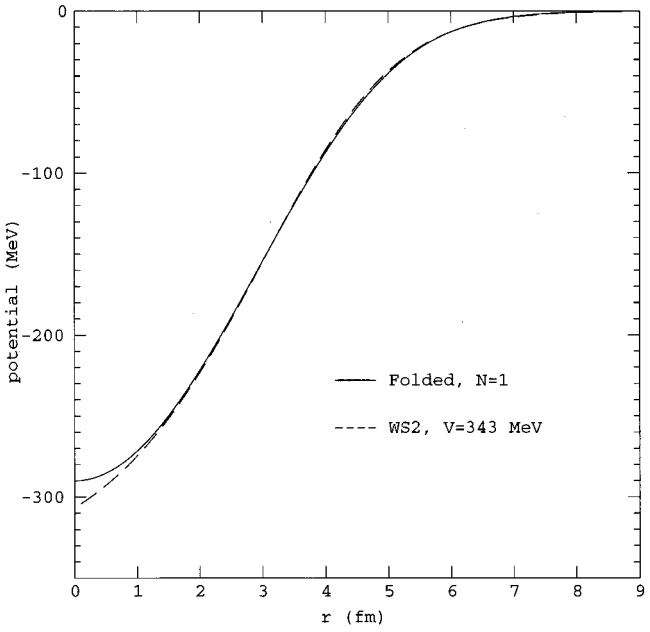

FIG. 1. Comparison of the folded potential (with $N=1$) with a Woods-Saxon-squared (WS2) one with $R_V=4$ fm and $a_V=1.4$ fm, and a depth $V=343$ MeV, chosen to have the same volume integral of $J_V=366$ MeV fm^3 as the folded one.

An analogous volume integral J_W for the imaginary potential can be obtained by substituting $W(r)$ in the above Eq. (1).

B. Folding model

Our understanding of the deep real parts of the optical potentials needed to describe light heavy-ion scattering is largely based upon the folding model, in which a realistic nucleon-nucleon effective interaction is folded over the distributions of nucleons within the two ions. Some account has to be taken of the exchange of the two interacting nucleons, which arises from antisymmetrizing the system. The resulting potential then represents the leading term in the Feshbach expression for the interaction of the two ions [2,13].

We use a density-dependent effective nucleon-nucleon interaction, called BDM3Y1, which is based upon the Paris nucleon-nucleon force and which has been developed recently, together with a realistic treatment of the exchange terms [14–16]. This has been shown to give a good account of light heavy-ion scattering at higher energies, as well as properties of $^{12}C+^{12}C$ scattering at low energies [10]. It also accounts for the saturation properties of cold nuclear matter. The density distributions of the two ions are described by two-parameter Fermi forms, with radii 2.60 fm (^{16}O) and 2.115 fm (^{12}C), and a surface diffuseness 0.45 fm for both. These values are in agreement with the rms charge radii deduced by the electron-scattering studies [17].

The resulting folded potentials have a weak dependence on energy, mostly arising from the exchange terms. The shape varies insignificantly with energy, so we adopted the potential evaluated at 124 MeV (the highest energy in the present work) as our standard. Then the theoretical potential

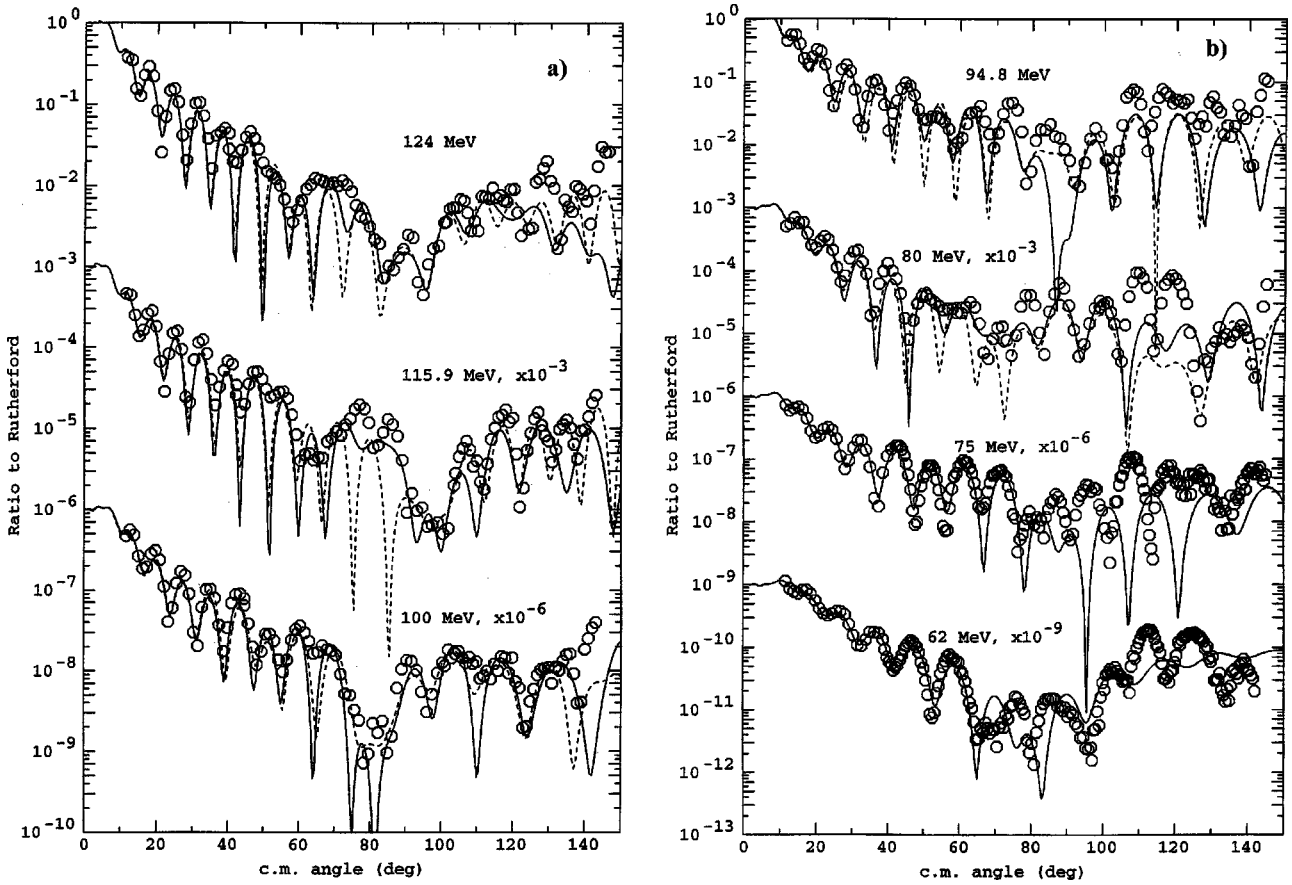

FIG. 2. Comparison of the measured cross sections (in ratio to the Rutherford cross sections) with the theoretical cross sections obtained with the WS2 potentials of Table I. In those cases where two alternative potentials are listed for a given energy, the solid curve corresponds to the first entry, and the dashed curve corresponds to the second one.

at 62 MeV (the lowest energy studied here) is *predicted* to be only 3% stronger. In practice we use the folded potential for 124 MeV times a normalization factor N, adjusted to optimize the fit to the data. N should be close to unity for this procedure to be meaningful.

C. Woods-Saxon real potentials

The Woods-Saxon shape provides a simple analytic form for the real potential. Indeed, parameters for the square of this form (WS2),

$$V(r) = -V f_V(r)^2, \tag{5}$$

where

$$f_V(r) = \left[1 + \exp\left(\frac{r - R_V}{a_V}\right)\right]^{-1}, \tag{6}$$

can be chosen to give a shape that is very close to the folded potential (except for radii less than about 1 fm which have little effect on the scattering). In the present case, a radius of $R_V = 4$ fm and a diffuseness of $a_V = 1.4$ fm give a potential very similar to the folded one (see Fig. 1). Equivalent fits to the data can be found with either the folded or the WS2 potentials. Furthermore, when the R_V and a_V parameters are allowed to vary from these values, they generally deviate very little and with only small changes in the value of χ^2. Consequently, we chose to adopt this WS2 potential as a standard one, varying only its strength V.

D. Spline model of the real potential

Spline potentials are defined by their values at certain radial knots, with cubic spline interpolation between them. The values at the radial knots, or a certain subset of them, are treated as the variables in a search. We chose the ten knots to be at $r = 1$ (1)10, and applied this model to the real potential. The imaginary potential was taken to be given by Eq. (2), as before. The additional adjustable parameters almost guarantee a better fit. The hope here was that this procedure would indicate any systematic deficiency in the folded or WS2 shapes. However, while somewhat better fits could be obtained at the higher energies with spline potentials that did not deviate strongly from the WS2 or folded ones, this was not the case at the lower energies where quite violent oscillatory deviations were indicated by the automatic search procedure. This was taken to indicate the presence of features that could not be represented by a smooth, local, and L-independent optical potential.

TABLE I. Potentials with Woods-Saxon-squared (WS2) real parts with $R_V=4$ fm and $a_V=1.4$ fm.

Energy [a] (MeV)	V (MeV)	J_V (MeV fm^3)	W (MeV)	R_W (fm)	a_W (fm)	W_D (MeV)	R_D (fm)	a_D (fm)	J_W (MeV fm^3)	J_{sur} (MeV fm^3)	J_{vol} (MeV fm^3)	σ_R [b] (mb)
124 [c]	296	316	14.5	4.258	0.131	9.2	5.973	0.453	64	40	25	1513
124 [d]	301	322	30.0	2.819	0.750	8.5	6.076	0.437	61	36	25	1527
115.9 [c]	288	308	15.7	4.378	0.090	7.0	6.089	0.461	61	32	29	1507
115.9 [d]	294	316	37.9	2.548	0.602	8.8	6.067	0.413	57	35	21	1473
100 [e]	302	323	14.0	4.363	0.001	7.2	6.171	0.421	56	31	25	1464
100	289	308	10.3	5.319	0.149	3.8	6.640	0.437	53	19	34	1530
94.8 [e]	285	304	11.3	5.231	0.127	3.5	6.725	0.360	51	15	36	1452
94.8	303	324	22.6	4.242	0.042	6.5	6.067	0.370	61	23	38	1352
80 [f]	290	309	13.6	4.915	0.076	3.1	6.276	0.427	49	14	35	1337
80 [g]	287	307	12.2	4.952	0.144	2.8	6.558	0.461	47	15	33	1428
75	305	326	11.7	5.147	0.072	4.4	6.566	0.304	50	15	35	1331
62 [h]	298	318	78.7	4.881	0.093	3.9	6.547	0.361	216	16	200	1290

[a]The ^{16}O laboratory energy.
[b]The total reaction cross section.
[c]The solution with small a_W.
[d]The solution with large a_W.
[e]This solution has an imaginary part which more closely follows the systematics (see Fig. 3).
[f]Obtained using statistical uncertainties.
[g]Obtained using uniform uncertainties.
[h]The parameters are poorly determined at this energy.

IV. RESULTS OF OPTICAL MODEL ANALYSES

The usual χ^2 criterion was used to judge the quality of agreement with the data, where

$$\chi^2=\frac{1}{N_\sigma-N_p}\sum_{i=1}^{N_\sigma}\frac{(\sigma_{\rm th}-\sigma_{\rm ex})^2}{(\Delta\sigma_{\rm ex})^2}, \tag{7}$$

where $\sigma_{\rm th}$, $\sigma_{\rm ex}$, and $\Delta\sigma_{\rm ex}$ are the theoretical cross sections, the experimental cross sections, and the uncertainties in the experimental cross sections, respectively. N_σ is the total number of angles at which measurements were made and N_p is the number of free fitting parameters. The fits were obtained using the automatic search option in the program PTOLEMY [18].

Two choices for the cross section uncertainties were considered. The first was to use the statistical uncertainties associated with the measurements. At the highest energies, these tend to weight the larger angles more heavily, while at the lower energies they weight more the smaller angles, or some combination.

In previous work, it has been common to use uniform uncertainties at all angles. This was done because the experimental uncertainties in those cases usually were smallest for the small angles, and it was felt that this gave too little importance to the large angles where the evidence for refractive effects was most likely to be seen. However, in the present case we anticipate the most difficulty in fitting the large angles and we wished to avoid biasing the searches to fit these angles at the expense of poorer fits at the forward angles. Studies showed this to be a real danger for the data at the higher energies. Consequently, after some experience we arrived at a compromise, presenting here results from using uniform (10%) uncertainties for the four highest energies, the statistical uncertainties for the data at 75 and 62 MeV, and both choices at 80 MeV.

A. WS2 potential results

After verifying that there was no evident need to allow the radius and diffuseness of the real potential to vary freely, we froze these quantities at the values $R_V=4$ fm and $a_V=1.4$ fm, and only allowed the depth V and the parameters of the imaginary potential to be varied for the optimum fit to the data. The resulting fits are shown in Fig. 2 and the corresponding parameter values are given in Table I, along with the associated volume integrals and the predicted reaction cross sections.

As anticipated, there is no difficulty in reproducing the forward diffractionlike structure in the angular distributions. However, the fits at larger angles, while suggestive, only reproduce the observed structure in a qualitative way. An overall increase in cross section at these angles is predicted (although often by not as much as seen experimentally), together usually with the same number of oscillations as observed. (It was determined that varying the radius and diffuseness of the real potential did not remedy these deficiences.)

The addition of a surface (WSD) imaginary term seems to be important; omitting it results in too little structure at the largest angles. Some trends in the parameter values can be seen. The real depths V correspond to real volume integrals J_V of about 310 ± 10 MeV fm^3, which are compatible with the values found for other systems in this energy region [2]. The volume (WS) term in the imaginary potential has a smaller radius than the surface term. At the highest energy of

124 MeV, fits could be found in which the diffuseness of this volume term is either large or small (see Table I, for examples). At 115.9 MeV, solutions could be found with either large or small a_W with similar χ^2 values, but subjectively the small a_W was judged much superior. No such ambiguity seems to exist at the lower energies; a very small value for a_W seems to be required. These values may be compared with the reduced wavelengths $\lambda\!\!\!^{-}$, which range from 0.24 to 0.34 fm in the present case, although the *local* wavelengths within the attractive potential will be somewhat shorter. It is true that a_W could be fixed arbitrarily at some small value, such as 0.1 fm, without much change, but we chose to quote the values resulting from the automatic search. As a result, the total imaginary potential has an almost square profile with a surface peak outside. Some typical examples are illustrated in Fig. 3.

B. Folding model results

As indicated earlier, the theoretical folded potential appropriate for a bombarding energy of 124 MeV was used at all energies. We have already remarked that our adopted WS2 potential ($R_V=4$, $a_V=1.4$) is very similar in shape to the folded one (see Fig. 1), so it is not surprising that we find fits with the folded real potential that are equivalent to those obtained with the WS2 version just discussed. Comparisons with the data are very similar to those shown in Fig. 3 for the WS2, so they are not shown here. The optimum values for the renormalizing factor N and the imaginary potential parameters are given in Table II, together with the associated volume integrals and the predicted reaction cross sections. The N values range from 0.83 to 0.89, except at 62 MeV where its value is rather poorly determined. However, even here a value $N=0.87$, fixed to give the same volume integral as the WS2 fit and more in line with the other energies, was shown to give an equally acceptable fit. The same ambiguity in a_W at the two highest energies is also found here, while the volume integrals of the imaginary potentials show the same kind of behavior (including being anomalously large at 62 MeV) as those associated with the WS2 real potentials.

C. Spline results

The imaginary potential was still represented by a sum of volume (WS) and surface (WSD) terms as in Eq. (2), but attempts were made to improve the agreement with the measured cross sections by using the more model-independent shapes for the real potential that are allowed by the spline procedure. It was hoped that these studies might reveal any systematic departures of the real potential from the folded shape that arise from higher-order corrections to the folding model. For example, such deviations could be expected to arise from the dispersion relation that connects the real and imaginary parts of the potential [2]. Then the existence of a prominent surface component in the imaginary potential, such as indicated here and which is itself a consequence of higher-order corrections to the optical potential, would result in a corresponding surface correction to the real potential. This spline approach still has limitations, however; for example, it is still local and does not allow any explicit L dependence which, in principle, would arise from these correction terms.

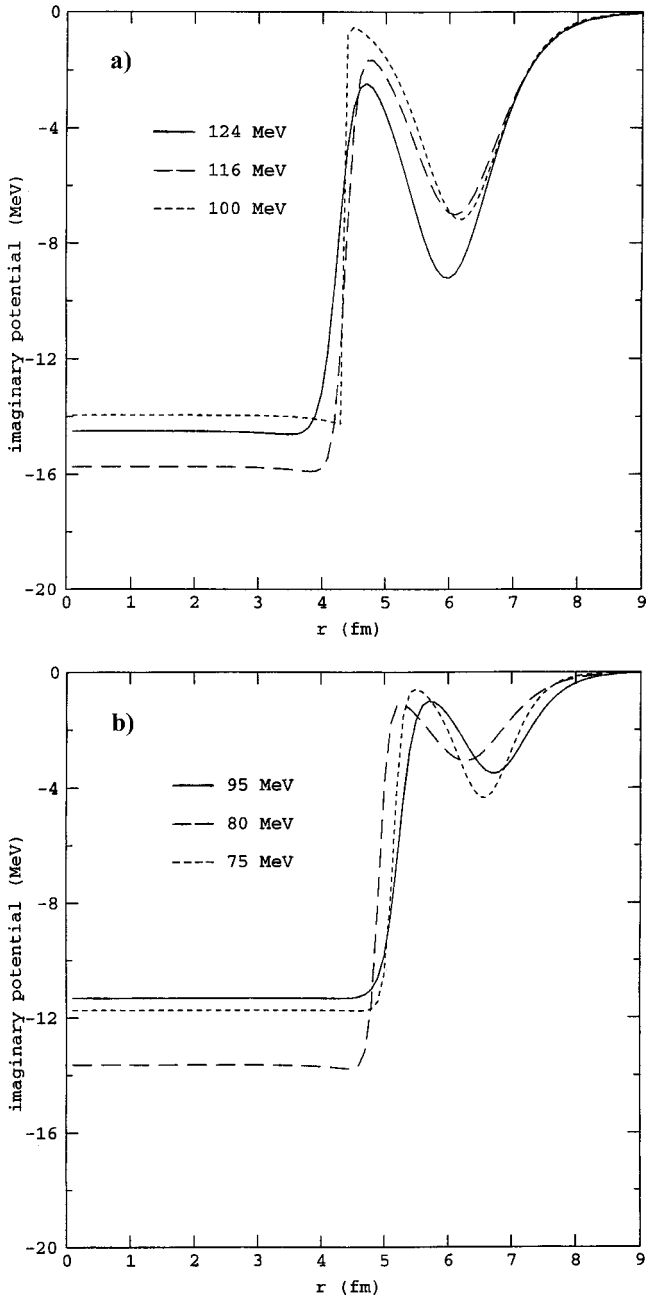

FIG. 3. The imaginary potentials associated with the WS2 potentials of Table I (except for the energy of 62 MeV). Where two alternatives are given in Table I, the curves correspond to the first choice.

The experimental statistical cross section uncertainties were used when applying this spline technique. Generally, the searches were initiated using starting values for the potential that were close to the folded one. Large reductions in the χ^2 values could be obtained with a variety of solutions. If one takes as a criterion that the spline potential should be physically reasonable, that is, it should not differ from the folded one too violently, an example could be found at each

TABLE II. Potentials obtained using the folded real part times *N*.

Energy (MeV)	*N*	J_V (MeV fm^3)	*W* (MeV)	R_W (fm)	a_W (fm)	W_D (MeV)	R_D (fm)	a_D (fm)	J_W (MeV fm^3)	J_{sur} (MeV fn^3)	J_{vol} (MeV fm^3)	σ_R (mb)
124	0.86	316	14.7	4.329	0.186	8.6	6.031	0.458	65	38	26	1520
115.9	0.85	311	16.4	4.336	0.089	7.0	5.986	0.468	59	30	29	1474
100	0.84	308	10.3	5.316	0.148	3.7	6.611	0.453	54	20	34	1527
94.8	0.83	304	11.3	5.206	0.127	3.6	6.663	0.376	51	16	35	1443
80	0.84	308	13.5	4.931	0.078	2.9	6.254	0.449	49	14	35	1330
75	0.89	326	9.6	5.281	0.091	2.9	6.731	0.356	43	12	31	1362
62 [a]	0.96	353	213	4.767	0.141	2.9	6.618	0.388	521	13	508	1299

[a]The parameters are poorly determined at this energy.

energy except at 62 MeV. These do not necessarily correspond to the lowest χ^2, nor do they necessarily reproduce all the details of the measured angular distributions. They are compared to the data in Fig. 4, and the real spline potentials are shown in Fig. 5. The associated imaginary potential parameters, etc., are given in Table III. The imaginary potentials have the same characteristics as were found when using the WS2 or folded real potentials, namely an almost square volume part (small a_W) with a surface peak outside.

V. DISCUSSION OF RESULTS

We have seen that the overall behavior of the measured cross sections can be reproduced by optical potentials with deep real parts (see Figs. 1 and 5, for example), whose shape is given by the folding model, or an equivalent Woods-Saxon-squared form. The strengths of these real potentials correspond to volume integrals J_V of 310 ± 10 MeV fm^3, with no evidence of dependence on energy in the region sampled here. Such values are close to (although somewhat

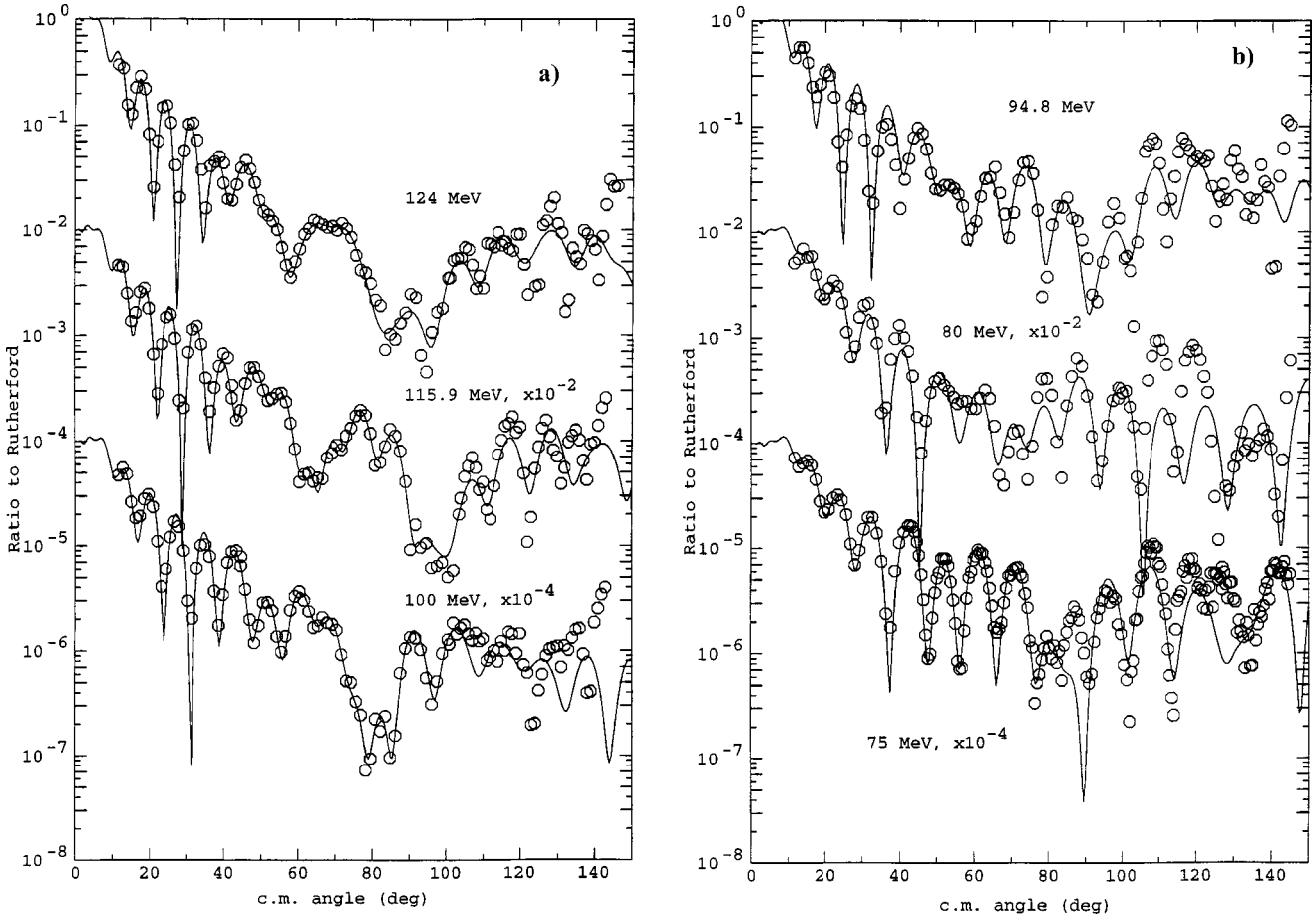

FIG. 4. Comparison with the measured cross sections of the cross sections predicted by the spline real potentials, which are shown in Fig. 5.

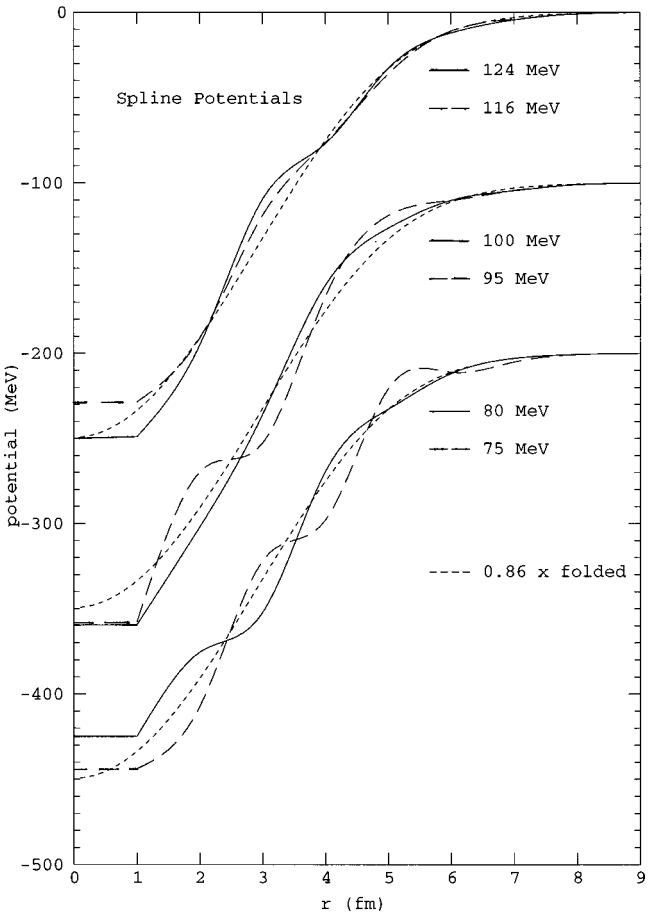

FIG. 5. The spline real potentials obtained, corresponding to the fits shown in Fig. 4.

smaller than) those predicted using a recently derived effective nucleon-nucleon interaction [14–16]. A renormalization factor N of about 0.86 ± 0.03 is required. They are also similar to the values found for the adjacent systems $^{12}C + ^{12}C$ and $^{16}O + ^{16}O$ at similar energies, as well as showing continuity with those found at much higher energies [2].

The associated imaginary potentials also display a consistent behavior, seeming to be driven by the data to have an almost square ''volume'' term, together with a ''surface'' term peaked at larger radii. One can understand how reflections from such a profile might introduce subsidiary scattering amplitudes whose interferences could produce the kind of structure observed in the angular distributions at large angles. Of course, one cannot tell whether this corresponds to reality or is merely a device for producing structure whose true origin may be quite different. An analysis of the amplitudes, such as by the semiclassical techniques of McVoy *et al.* [19,20], could be helpful here. Within our restriction to local, L-independent potentials, this type of imaginary part was the only one which would give a consistent description of the data at all energies. However, one is tempted to speculate about a simple interpretation of this imaginary part, and identify the volume term with absorption due to fusion and associated processes, and the surface term with more direct reactions. In the tables we show separately the contributions of these two terms to the volume integral of the imaginary potential. It is interesting that the volume term decreases only slowly as the energy decreases (the anomalously large value at 62 MeV is poorly determined and is presumably due to our inability to obtain a good description of the data at this energy), whereas the surface contribution is reduced by a factor of 2 or more when the energy drops to 62 MeV. The latter behavior might be expected for direct, surface-type reactions as the energy falls. Furthermore, the radii R_D of the surface peak fall between 6 and 7 fm, just inside the ''strong absorption radius.'' (If this is defined as the distance of closest approach on a Rutherford orbit with the angular momentum for which the transmission coefficient is one-half, its value ranges from 7.4 fm at 124 MeV to 7.8 fm at 62 MeV.)

The analyses using the spline form for the real potential resulted in better agreement with the measurements, especially at the large angles, although the improvement found at 62 MeV was quite minor and the potential itself deemed to be unphysical. It is difficult to judge the physical significance of these results, except to say that relatively small and oscillatory departures of the real potential from the smooth WS2 or folded shape usually can result in considerably improved agreement with the data (as judged by the χ^2 criterion). It is also difficult to discern any systematics in these deviations, except to note some similarities between those at 124 and 115.9 MeV, and between those for 94.8 and 80 MeV, while those for 100 MeV appear to be intermediate.

The various optical potentials that we have obtained also qualify as relatively weakly absorbing, hence allowing the

TABLE III. Imaginary potential parameters and volume integrals associated with the use of the spline model for the real potential.

Energy (MeV)	J_V (MeV fm^3)	W (MeV)	R_W (fm)	a_W (fm)	W_D (MeV)	R_D (fm)	a_D (fm)	J_W (MeV fm^3)	J_{sur} (MeV fm^3)	J_{vol} (MeV fm^3)	σ_R (mb)
124	313	12.4	4.964	0.165	6.0	6.084	0.447	60	33	27	1498
115.9	316	13.0	5.002	0.158	4.7	6.197	0.399	55	19	36	1422
100	313	11.2	5.057	0.192	4.2	6.266	0.383	49	17	32	1402
94.8	294	13.6	4.413	0.160	2.8	6.321	0.459	39	14	26	1395
80	316	14.5	4.930	0.080	3.1	6.309	0.419	52	14	38	1331
75	325	8.3	4.722	0.169	7.0	6.256	0.265	39	19	19	1304
62 [a]	322	24.7	4.874	0.050	5.7	6.499	0.275	80	17	62	1285

[a]The parameters are poorly determined at this energy.

scattering to be sensitive to the potential at small distances [2]. A measure of this is given by the magnitude of the *S*-matrix element for the low partial waves. In the present case the magnitudes for the *S* wave range from 0.02 to 0.04, much larger than would be encountered in truly strong-absorption scattering, which typically might be 10^{-4}.

The predicted reaction cross sections associated with these potentials show a steady decrease from about 1.5 b at 124 MeV to about 1.3 b at 62 MeV. These values are close to, but somewhat larger than, those expected from other work on this system [21]. The result at 124 MeV is consistent with a more recent analysis of data at 132 MeV [4].

Finally, we note that a real potential very similar to that found here has been proposed [22] to explain the oscillations with respect to energy observed in the fusion cross sections for $^{16}O+^{12}C$ over the energy range of $12 \leqslant E_{c.m.} \leqslant 39$ MeV, which partially overlaps the energy range considered here. Also, the results of a recent analysis [23] of $^{16}O+^{16}O$ elastic scattering data in the same energy interval studied here are consistent with the conclusions reached in the present study.

ACKNOWLEDGMENTS

S.S. and Z.B. want to express their gratitude to the Institut de Recherches Subatomiques, Strasbourg, for the warm hospitality during their stay. The work at Universidad Nacional Autónoma de México was partially supported by CONACYT 3039PE. Theoretical nuclear physics research at the University of Tennessee is supported by the U.S. Department of Energy through Contracts No. DE-FG05-93ER40770 and DE-FG05-87ER40461. Oak Ridge National Laboratory is managed by Lockheed Martin Energy Research Corporation for the U.S. Department of Energy under Contract No. DE-AC05-96OR22464. S.S. acknowledges financial support through the French Embassy in Zagreb.

[1] M.E. Brandan, M.S. Hussein, K.W. McVoy, and G.R. Satchler, Comments Nucl. Part. Phys. **22**, 77 (1996).
[2] M.E. Brandan and G.R. Satchler, Phys. Rep. **285**, 143 (1997).
[3] M.E. Brandan, A. Menchaca-Rocha, M. Buenerd, J. Chauvin, P. De Saintignon, G. Duhamel, D. Lebrun, P. Martin, G. Perrin, and J.Y. Hostachy, Phys. Rev. C **34**, 1484 (1986).
[4] A.A. Ogloblin, Dao T. Khoa, Y. Kondō, Yu.A. Glukhov, A.S. Dem'yanova, M.V. Rozhkov, G.R. Satchler, and S.A. Goncharov, Phys. Rev. C **57**, 1797 (1998).
[5] K.A. Erb and D.A. Bromley, in *Treatise on Heavy-Ion Science*, Vol. 3, edited by D.A. Bromley (Plenum, New York, 1984).
[6] A. Morsad, F. Haas, C. Beck, and R. M. Freeman, Z. Phys. A **338**, 61 (1991).
[7] S. Szilner, Z. Basrak, R.M. Freeman, F. Haas, A. Morsad, and C. Beck, Phys. Rev. C **55**, 1312 (1997).
[8] S. Szilner, Z. Basrak, R.M. Freeman, F. Haas, A. Morsad, M.P. Nicoli, and C. Beck, J. Phys. G: Nucl. Part. Phys. **25**, 1927 (1999).
[9] K.W. McVoy and M.E. Brandan, Nucl. Phys. **A542**, 295 (1992).
[10] Y. Kondō, M.E. Brandan, and G.R. Satchler, Nucl. Phys. **A637**, 175 (1998).
[11] M.P. Nicoli, Thèse de Doctorat de l'Université Louis Pasteur de Strasbourg (1998); IReS Report 98-16.
[12] W. von Oertzen and H.G. Bohlen, Phys. Rep. **19**, 1 (1975).
[13] H. Feshbach, *Theoretical Nuclear Physics* (Wiley, New York, 1992).
[14] Dao T. Khoa and W. von Oertzen, Phys. Lett. B **304**, 8 (1993).
[15] Dao T. Khoa, W. von Oertzen, and H.G. Bohlen, Phys. Rev. C **49**, 1652 (1994).
[16] Dao T. Khoa *et al.*, Phys. Rev. Lett. **74**, 34 (1995).
[17] H. de Vries, C.W. de Jager, and C. de Vries, At. Data Nucl. Data Tables **36**, 495 (1987).
[18] M.H. Macfarlane and S.C. Pieper, Argonne National Laboratory report ANL-76-11 (1978).
[19] S.H. Fricke, M.E. Brandan, and K.W. McVoy, Phys. Rev. C **38**, 682 (1988).
[20] M.E. Brandan, K.W. McVoy, and G.R. Satchler, Phys. Lett. B **281**, 185 (1992).
[21] M.E. Brandan and A. Menchaca-Rocha, Phys. Rev. C **23**, 1272 (1981).
[22] C. Gao and Y. Kondō, Phys. Lett. B **408**, 7 (1997).
[23] M.P. Nicoli *et al.*, Phys. Rev. C **60**, 064608 (1999).